ACS OMEGA

http://pubs.acs.org/journal/acsodf

Article

Ternary Metal (Cu−Ni−Zn) Oxide Nanocomposite via an Environmentally Friendly Route

Jahanzeb Khan,* Saiqa Bibi, Irsa Naseem, Shakeel Ahmed, Muhammad Hafeez, Khalil Ahmed, Faizah Altaf, Davoud Dastan,* Asad Syed,* Majid S. Jabir, Mustafa K. A. Mohammed,* and Lin Tao

Cite This: *ACS Omega* 2023, 8, 21032−21041

Read Online

ACCESS | Metrics & More | Article Recommendations

ABSTRACT: In this work, we report the engineering of sub-30 nm nanocomposites of CuO/ZnO/NiO by using *Dodonaea viscosa* leaf extract. Zinc sulfate, nickel chloride, and copper sulfate were used as salt precursors, and isopropyl alcohol and water were used as solvents. The growth of nanocomposites was investigated by varying the concentrations of precursors and surfactants at pH 12. The as-prepared composites were characterized by XRD analysis and found to have CuO (monoclinic), ZnO (hexagonal primitive), and NiO (cubic) phases with an average size of 29 nm. FTIR analysis was performed to investigate the mode of fundamental bonding vibrations of the as-prepared nanocomposites. The vibrations of the prepared CuO/ZnO/NiO nanocomposite were detected at 760 and 628 cm^{-1}, respectively. The optical bandgap energy of the CuO/NiO/ZnO nanocomposite was 3.08 eV. Ultraviolet−visible spectroscopy was performed to calculate the band gap by the Tauc approach. Antimicrobial and antioxidant activities of the synthesized CuO/NiO/ZnO nanocomposite were investigated. It was found that the antimicrobial activity of the synthesized nanocomposite increases with an increase in the concentration. The antioxidant activity of the synthesized nanocomposite was examined by using both ABTS and DPPH assays. The obtained results show an IC_{50} value of 0.110 for the synthesized nanocomposite compared to DPPH and ABTS (0.512), which is smaller than that of ascorbic acid (IC_{50} = 1.047). Such a low IC_{50} value ensures that the antioxidant potential of the nanocomposite is higher than that of ascorbic acid, which in turn shows their excellent antioxidant activity against both DPPH and ABTS.

1. INTRODUCTION

Nanoparticles as well as multifunctional nanomaterials have diverse applications in various fields such as catalysis,[1,2] wastewater treatment, bioimaging, cancer therapy, etc. Trimetallic NPs have enhanced applications as well as selectivities compared to bi- and monometallic nanoparticles. Because of their wide range of applications, a wide range of preparation routes such as physical,[3−5] chemical,[6−14] and biological[15] methods have all been used to synthesize NPs, with the biological method being recognized as the most environmentally friendly and the other methods having serious drawbacks.[16] Drug-resistant bacteria have recently been a main cause of various infectious diseases and death around the world.[17] Free radicals of various chemical origins are highly unstable; removal of electrons from other molecules to achieve equilibrium resulted in molecular breakdown. Such extremely reactive species continuously develop inside the human body, and they can damage short-lived chemicals and cellular components such as DNA, lipids, and protein.[18] When an electron or hydrogen ion is accepted, $ABTS^{\bullet+}$ becomes a stable free radical, which forms stable molecules. The adverse effects of free radicals include heart diseases, cancer, and neurological illnesses. This can be reduced by scavenging these radicals.[19] As a result, there is an urgent need to come up with some practical solutions to this major global issue. Because of their unique physicochemical features, nanomaterials have gained considerable attention from researchers. Because of their wide range of applications, the commercial uprising resulted in the manufacture of hundreds of nanomaterials.[20] The electronic, optical, and magnetic properties of multimetallic NPs are diverse. The properties of multimetallic NPs, such as their large surface area, size, shape, and ζ potential, allow them to interact efficiently with bacterial cell membranes, causing disruption, ROS production, protein destruction, DNA damage, and

Received: March 21, 2023
Accepted: May 11, 2023
Published: June 2, 2023

https://doi.org/10.1021/acsomega.3c01896
ACS Omega 2023, 8, 21032−21041

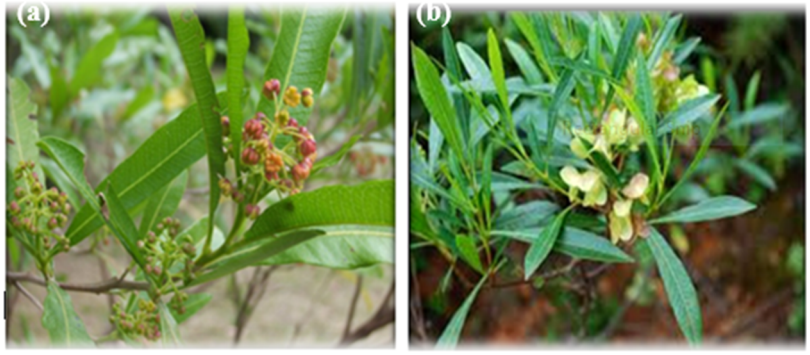

Figure 1. Pictorial illustration of the plant *Dodonaea viscosa:* (a) side view and (b) top view.

eventually death, which is aided by the host immune system.[21,22]

Plant extracts and bacteria are utilized in biological techniques to synthesize nanoparticles.[23] Photonanotechnology is a new cost-effective, environmentally friendly, and easy process to synthesize nanoparticles.[24] Plant parts such as leaves,[25] roots,[26] fruits,[27] and seeds[28] are used to synthesize nanoparticles in this technology. Second, metabolites found in plants, such as polysaccharides, heterocyclic compounds, terpenoids, various types of organic acids, alkaloids, vitamins, and proteins, are combined to synthesize nanoparticles.[29] Researchers have long been interested in the biological applications of metal oxide nanoparticles such as copper oxide, zinc oxide, and nickel oxide.[30] Sudha et al. studied the effects of a copper device on three different bacterial strains, including *E. coli*, *Vibrio cholerae*, and *Salmonella typhi*.[31] The cytotoxic and antioxidant effects of ZnO nanoparticles made from *Mangifera indica* leaves were tested on lung cancer cells. When the amount of ZnO nanoparticles was increased, the antioxidant activity of the particles increased. The DPPH technique was employed to investigate the antioxidant activity of ZnO nanoparticles, and the antioxidant activity of ZnO was shown to be comparable to that of ascorbic acid.[32]

Pure nanoparticles of various metal oxides, such as ZnO, CuO, and Fe_2O_3, were fabricated using the sol−gel method.[33−37] Moreover, the antibacterial activity of these three metal oxide nanoparticles was investigated using a range of bacteria. The antibacterial activities of these three metal oxide nanoparticles vary as the surface-to-volume ratio changes. The results revealed that ZnO nanoparticles had the highest bacterial activity among the three metal oxide nanoparticles tested.[38]

In the current study, *Dodonaea viscosa* leaf extracts were employed to synthesize CuO/ZnO/NiO nanoparticles due to their diverse catalytic, food-packing, wastewater treatment, and biological applications. *Dodonaea* comprises one of the largest genera in the Sapindaceae family, which contains 70 species widely distributed in continental Australia. Among these, *Dodonaea viscosa* is considered to be one of the world's most widely disseminated transoceanic plants.[39] It was traditionally used to treat skin infections as well as hepatic and spleen pain. Its leaves are used to cure fractures and as an anti-inflammatory, antioxidant, antibacterial, and antifungal agent.[40] Photochemical research on *Dodonaea viscosa* revealed that it is a rich source of phenolic compounds, saponins, ascorbic acid, and steroids. These chemicals exhibit a high level of antioxidant activity.[41] The *D. viscosa* leaf extract is used by researchers to synthesize nanocomposites due to its traditional medicinal properties,[41] potential for green synthesis,[26] and unique phytochemical profile.[27] We are interested in exploring a novel and unexplored avenue for nanocomposite synthesis. The antioxidant and antibacterial properties of the synthesized nanocomposite were investigated in the current study. To the best of our knowledge, this is the first report in which a ZnO/CuO/NiO ternary metal oxide nanocomposite has been synthesized by using the said plant, with enhanced biological applications.

2. EXPERIMENTAL SECTION

2.1. Materials. Zinc sulfate, nickel chloride, and copper sulfate were used as salt precursors. Sodium hydroxide was used to maintain the pH of the solutions. Distilled water was utilized to prepare solutions. DPPH and ABTS were used to determine the antioxidant activity of the nanocomposite. All chemicals were purchased from Sigma-Aldrich. *Dodonaea viscosa* leaf extract was used as the stabilizing agent. Furthermore, bacterial strains such as GPB (*S. aureus*) and GNB (*E. coli*) were obtained from the Department of Biotechnology, AJK University, Muzaffarabad, Pakistan.

2.2. Preparation of Plant Leaf Extract. *Dodonaea viscosa* leaves were collected from AJK (Muzaffarabad city). Figure 1a,b shows images of the *Dodonaea viscosa* plant. For the preparation of the leaf extract of *D. viscosa*, the leaves were rinsed with tap water and washed with distilled water. Then, the leaves were shade dried for 7 days. After that, the dried leaves were ground into a fine powder. 5 g of leaves were added into 100 mL of distilled water and boiled at 80 °C for 3 h to prepare the leaf extract.

Then, the extract was filtered by Whatman filter paper 1, the filtrate was centrifuged, and the upper clear layer was used. The leaf extract was stored at 4 °C until further use. This method has been used for the extraction of essential oil,[42−44] seed oil,[45,46] and nanoparticle formation.[47−53]

2.3. Synthesis of the Ternary Metal (Cu−Ni−Zn) Oxide Nanocomposite. 50 mM solutions of zinc sulfate, copper sulfate, and nickel chloride were prepared. Only 80 mL was taken from each solution. After that, 20 mL of *Dodoanea viscosa* leaf extract was added to these three solutions and stirred constantly at 700 rpm and 80 °C. 2 M sodium hydroxide solution was added into each beaker to maintain the pH at 13. Reactions were carried out till precipitates appeared in the three beakers. Precipitate formation indicates the formation of zinc oxide, copper oxide, and NiO nanoparticles. Then, these three reactions were mixed and stirred constantly at 700 rpm and 80 °C for 5 h. A 2 M solution of sodium hydroxide was added every 20 min to maintain the pH at 13.

https://doi.org/10.1021/acsomega.3c01896
ACS Omega 2023, 8, 21032−21041

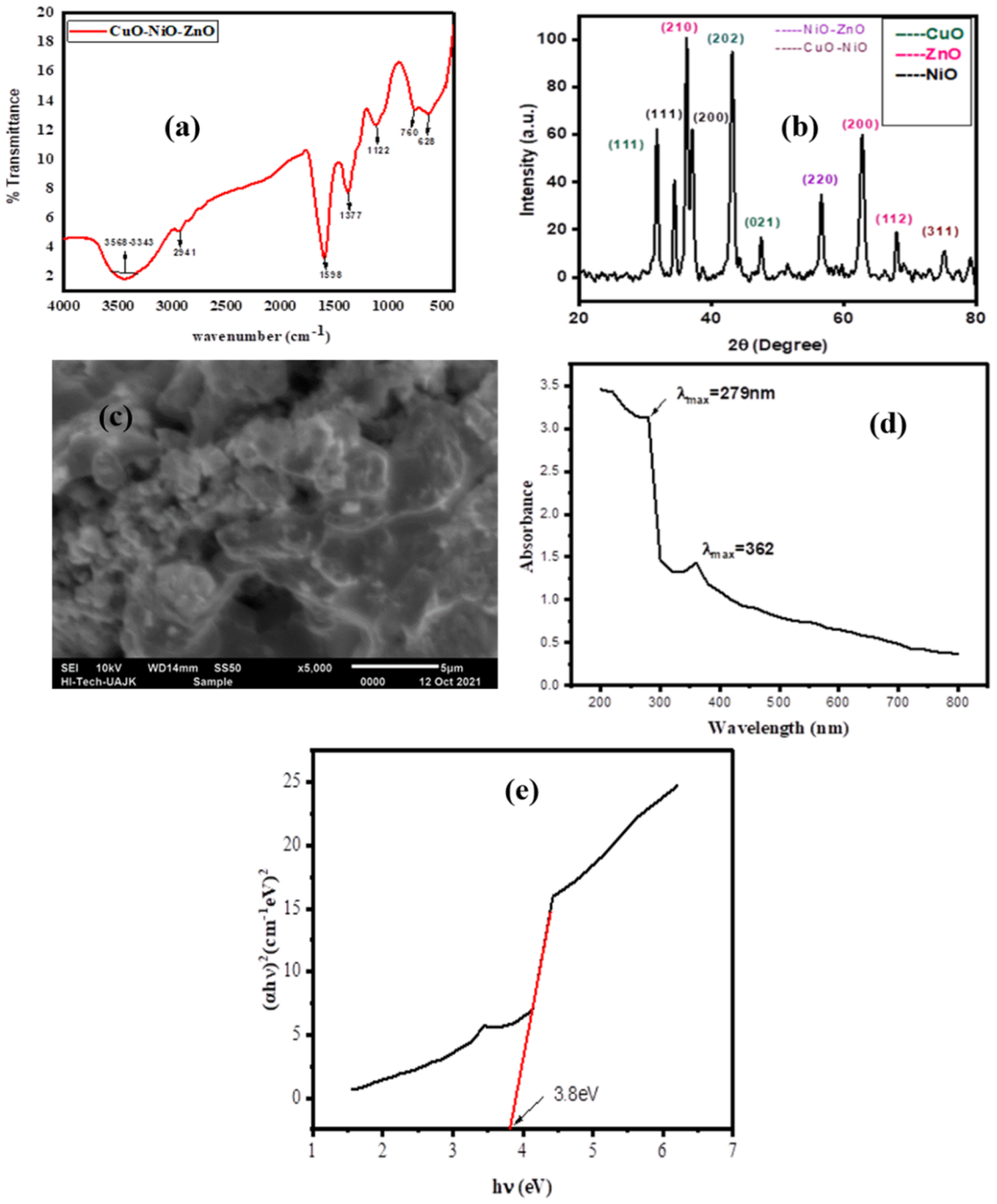

Figure 2. (a) FT-IR spectra, (b) XRD pattern, (c) SEM image, (d) UV−visible absorbance spectra, and (e) bandgap energy of the prepared nanocomposite.

After 5 h, the turbid reaction mixture was then aged for 24 h and then purified by centrifuging for 15 min at 3000 rpm. Then, the product obtained was washed with deionized water. Precipitates were dried and then converted into a fine powder with the help of a mortar and pestle. The powder was washed again using distilled water 3−4 times. Calcination was carried out at 350 °C.[54]

2.4. Antioxidant Activity. *2.4.1. Analytical Procedure (ABTS Assay).* The antioxidant activity of the CuO/ZnO/NiO nanocomposite was assessed via the ABTS radical-scavenging assay, which was slightly modified. The reduction of the radical cation $ABTS^{\bullet+}$ to ABTS (2,2-azinobis-(3-ethylbenzothiazoline-6-sulfonic) diammonium salt) causes the first decolonization. 7 mM ABTS and 2.5 mM potassium persulfate were stirred together and maintained in darkness for 16 h to form the $ABTS^{\bullet+}$ free radical for the preparation of the ABTS stock solution. The absorbance of this solution was evaluated at 734 nm (A_0) using a UV−visible double-beam spectrophotometer. Different concentrations of biologically synthesized nanocomposites (1, 3, 5, and 7 mg/mL) were analyzed against ABTS radical scavenging. The absorbance (A_i) was recorded, and the percentage scavenging potential was calculated using the formula given below. During the study, a standard (ascorbic acid) was employed.[41]

$$\%\text{RSA} = [(A_0 + A_i/A_0)] \times 100 \quad (1)$$

https://doi.org/10.1021/acsomega.3c01896
ACS Omega 2023, 8, 21032−21041

2.4.2. Analytical Procedure (DPPH Radical Assay). Different concentrations of biologically synthesized nanocomposites (1, 3, 5, and 7 mg/mL) were analyzed against DPPH in the radical-scavenging assay. A solution (0.2 mM) of DPPH was prepared in distilled methanol and incubated for 30 min in dark.[42] One milliliter of this solution was taken, and the absorbance was measured at 517 nm to serve as the blank (A_0). The absorbance (A_i) was recorded, and the percentage scavenging potential was calculated using the following formula:[43]

$$\%\text{RSA} = [(A_0 + A_i/A_0)] \times 100 \quad (2)$$

2.5. Antibacterial Activity. The synthesized CuO/NiO/ZnO nanocomposite was used to determine the antimicrobial activity. The bacteria used were obtained from the Department of Biotechnology, AJK University, Muzaffarabad, Pakistan. GPB (*S. aureus*) and GNB (*E. coli*) were used for this analysis. Nutrient agar was used to culture bacteria. The overnight bacterial culture was combined with fresh sterilized agar media and deposited into sterilized Petri plates, where it was solidified under a laminar flow. Each plate had 5 mm diameter wells. An ultrasonic dispersion was used to prepare several suspensions of the CuO/NiO/ZnO nanocomposite in distilled water, and then this ultrasonic suspension was placed into each well and incubated overnight. After 24 h, the activity of the NiO/CuO/ZnO nanocomposite was measured in millimeters surrounding each well to determine its activity. A standard reported method was used for testing.

3. RESULTS AND DISCUSSION

3.1. FT-IR Spectroscopy. Figure 2a depicts the FT-IR spectrum of the synthesized nanocomposite, which possesses a broad peak between 3568 and 3343 cm^{-1} possibly due to lattice water or atmospheric water.[55−57] The band at 2941 cm^{-1} is due to C−H stretching.[58] The peak at 1595 cm^{-1} is because of the aromatic C═C stretch. The peak at 1377 cm^{-1} shows that the compound is purely aromatic. The band at 1122 cm^{-1} demonstrates the C−O stretching vibrations.[47] The band for the M−O bond lies in the range of 1000−400 cm^{-1}, which is related to the CuO/NiO/ZnO nanocomposite. Therefore, the merged band at 760 and 628 cm^{-1} can be assigned to stretching and bending vibrations of the CuO/ZnO/NiO nanocomposite.[48]

3.2. X-ray Diffraction (XRD) Analysis. XRD was performed to determine the crystallite structure as well as the crystallite size of the synthesized nanocomposite. Figure 2b shows the XRD pattern of the synthesized nanocomposite of CuO/NiO/ZnO. The XRD pattern obtained has sharp and intense peaks, which confirm the highly crystalline nature of the synthesized nanocomposite.[49] The peaks with *hkl* values of (111) and (200) indicate a cubic geometry of the synthesized nickel oxide nanoparticles (JCPDS: 73-1523). The peaks at 2θ = 37.2, 63.5, and 68.1° indicate the hexagonal primitive phase of ZnO nanoparticles, having good agreement with JCPDS: 01-1136. The peaks at 2θ = 33.23, 48.9, and 56.8°, with *hkl* values of (111), (202), and (021), in good agreement with JCPDS: 65-2309, indicate the monoclinic geometry of CuO nanoparticles. The additional peaks at 2θ = 75.1 and 58.2° with *hkl* values of (311) and (220) were due to cubic phase CuO−NiO (JCPDS: 78-0648) and NiO−ZnO (JCPDS: 75-0270).[50] The average crystallite size of the synthesized CuO/ZnO/NiO nanocomposite was calculated by using the Debye Scherer formula[59−62]

$$D = 0.9\lambda/\beta \cos\theta \quad (3)$$

where λ is the X-ray wavelength, β is the full width at half-maximum of the peaks, and 0.9 is the value of the Scherer constant. The average crystallite size of the synthesized nanocomposites was found to be 29 nm by using the Scherer formula.

3.3. Scanning Electron Microscopy (SEM). Figure 2c shows the morphology of the synthesized CuO/NiO/ZnO nanocomposite. The SEM micrograph shows that the background was highly agglomerated, where cavities were also observed at certain points. At the surface of the complex structure, a few particles with visible boundaries were also seen. These individual particles were also irregular in shape.[63]

3.4. UV−Visible Spectroscopy. Figure 2d shows the absorption spectra of the CuO/NiO/ZnO nanocomposite. The UV−visible absorption spectra of the synthesized CuO/ZnO/NiO nanocomposite exhibited two absorption bands at 279 and 362 nm.[64] Figure 2e represents the Tauc plot of the CuO/ZnO/NiO nanocomposite. To determine the bandgap energy of the nanocomposite, a graph is plotted between $(\alpha h\nu)^2$ and $h\nu$.[65−67] The energy band gap of the synthesized nanocomposite was 3.8 eV.[68−76]

3.5. Biological Applications. *3.5.1. Antibacterial Activity.* Trimetallic nanocomposites have enhanced antibacterial activity compared with monometallic and bimetallic nanoparticles. As an example, the green synthesized Au−Pt−Ag nanocomposite exhibits efficient antimicrobial activity against *E. coli* and *S. aureus*.[77−79]

The antimicrobial activity of the synthesized CuO/NiO/ZnO nanoparticles against GPB (*S. aureus*) and GNB (*E. coli*) was tested using the agar well diffusion technique.[80−84] The antibacterial action of NPs is mediated by a variety of mechanisms. The production of reactive oxygen species (ROS) is the most significant. Then, these reactive species cause cell death by disturbing the respiratory cycle, the protein cycle, preventing or modifying DNA replication, and the food metabolism cycle.[57]

Table 1 shows the zone of inhibition against GPB, and GNB was evaluated via the agar well diffusion technique in millimeters around each well. PC represents the positive control (clindamycin), and NC represents the negative control (distilled water).

Table 1. Inhibition Zones In Millimeters of Nanocomposites against *S. aureus* and *E. coli*

	ZnO/CuO/NiO conc.					
bacteria	10 μg	20 μg	30 μg	40 μg	PC	NC
S. aureus	14	18	22	25	28	00
Escherichia coli	11	16	20	23	00	26

At different concentrations, 10, 20, 30, 40 μg/mL, the antibacterial activities of the produced CuO/ZnO/NiO nanocomposite were investigated. The antibacterial efficiency of the nanocomposite against two separate bacterial strains improved as its concentration was increased. This could be because of an increased number of reactive species capable of inhibiting bacterial growth.[58] Images of the antimicrobial activity of the CuO/ZnO/NiO nanocomposite are shown in Figure 3b. The results indicate that the synthesized nanocomposite had excellent antibacterial activity. The greatest

https://doi.org/10.1021/acsomega.3c01896
ACS Omega 2023, 8, 21032−21041

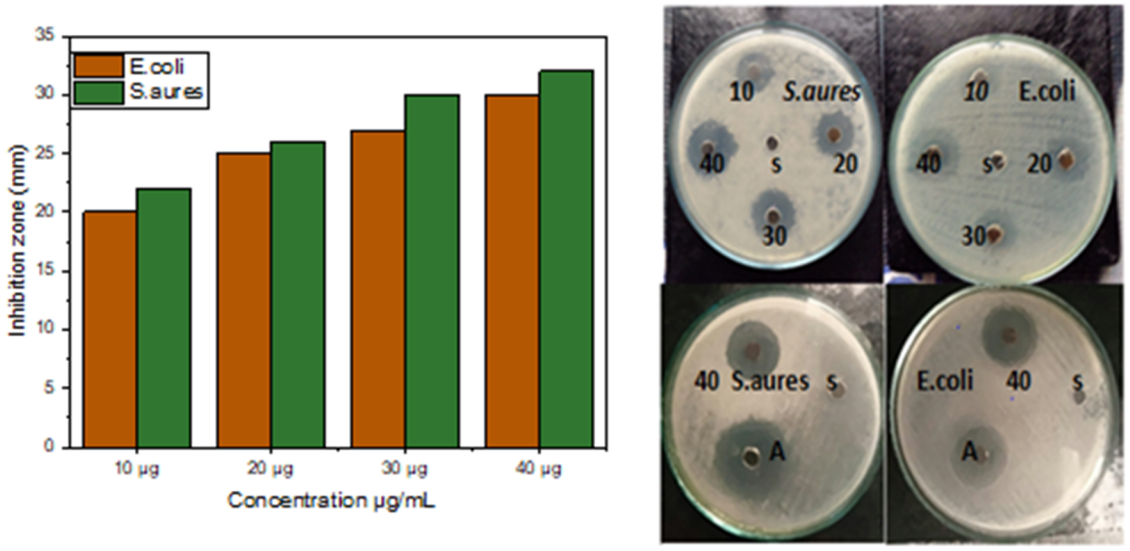

(a) (b)

Figure 3. (a) Images of antibacterial activity. (b) Comparison of the antibacterial activity of the nanocomposite against different strains.

zone of inhibition was observed against GPB at 40 μg/mL concentration.

The antimicrobial activity of the CuO/ZnO/NiO nanocomposite studied in this article was compared with previously reported data, which are presented in Table 2. It shows that

Table 2. Comparison of Antibacterial Activities of the Synthesized Nanocomposite With Data from Previously Reported Studies

sr. no.	NPs	synthesis method	inhibition zone diameter (mm)	refs
1	NiO	green synthesis via Stevia leaf extract	14	99
2	CuO	green synthesis via *Aerva javanica* extract	9	100
3	ZnO	green synthesis via *Cassia fistula* extract	14	101
4	CuO−ZnO	green synthesis via *Mentha longifolia* leaf extract	17	102
5	CuO−ZnO−NiO	green synthesis via *Dodonaea viscosa* extract	25	present study

the synthesized nanocomposite has higher antibacterial activity than previously reported single and bimetallic nanoparticles. Moreover, the CuO/ZnO/NiO nanocomposites reported earlier were tested only for antimicrobial activity, whereas the currently reported nanocomposite was tested for antimicrobial as well as antioxidant activities.[85−91]

Figure 3a indicates that the synthesized nanocomposite has better antibacterial activity against GPB (*S. aureus*) than GNB (*E. coli*). The reason is that the peptidoglycan layer of gram-positive bacteria is thick. As a result, attacking and damaging the bacterial cell wall is easier. The outer layer of gram-negative bacteria has excess lipopolysaccharides. As a result, strains have a higher charge as compared to GPB. Therefore, the mixed metal oxide CuO/NiO/ZnO is found to have a greater inhibitory impact against gram-positive bacteria.[92−98]

Gram-positive and gram-negative bacteria adopt different mechanisms to allow the CuO/ZnO/NiO nanocomposite inside the cell, which could be because of membrane composition differences. The attachment of the CuO/ZnO/NiO nanocomposite and its transport inside the bacterial cell membrane depend on the membrane composition.

3.5.2. Antioxidant Activity. Free radicals harm and mutate cells, which has an impact on human health. In order to eliminate ROS, antioxidants are necessary. The antioxidant activity of nanocomposites in vitro indicates their pharmacological function.[103−106] A recent study showed that the antioxidant activity of synthesized nanocomposites can be analyzed by various methods, but the ABTS assay and the DPPH radical assay are considered to be the most reliable methods.[107−109] The antioxidant activity of the biogenically synthesized nanocomposite against ABTS free radical cations was analyzed, and ascorbic acid was used as the standard. Initially, $ABTS^{\bullet+}$ free radical cations are formed due to the removal of electrons from nitrogen. ABTS is oxidized to create $ABTS^{\bullet+}$ by a variety of oxidizing agents such as potassium persulfate or manganese dioxide. After reacting with antioxidants, $ABTS^{\bullet+}$ decolorizes the solution.[16]

On the other hand, in the case of the DPPH assay, the DPPH radical is reduced by accepting an electron or hydrogen from the antioxidant species, resulting in a light yellow color and a substantial drop in the absorbance maximum.

The phytochemical analysis of *Dodonaea viscosa* revealed that it is a rich source of phenolic compounds, saponins, ascorbic acid, and steroids. These chemicals have outstanding antioxidant properties. Hence, the compounds present in the leaf extract enhanced the antioxidant activity of the synthesized nanocomposite.[28] The percentage radical-scavenging activity of the synthesized nanocomposite was investigated at different concentrations of 1, 3, 5, and 7 mg/mL. Tables 3 and 4 show that with an increase in concentration, the percentage scavenging of the synthesized nanocomposite against DPPH

https://doi.org/10.1021/acsomega.3c01896
ACS Omega 2023, 8, 21032−21041

Table 3. Percentage Radical-Scavenging Activity of the Nanocomposite against ABTS

concentration (mg/mL)	A_0	A_i	%RSA	IC_{50}
1	0.208	0.097	50	0.512
3	0.208	0.064	69	
5	0.208	0.043	79	
7	0.208	0.02	90	

Table 4. Percentage Scavenging Activity of the Nanocomposite against DPPH

concentration (mg/mL)	A_0	A_i	%RSA	IC_{50}
1	0.512	0.216	57	0.11
3	0.512	0.189	63	
5	0.512	0.098	81	
7	0.512	0.048	90	

as well as ABTS increases. In general, the test sample exhibited more %RSA of the DPPH radical than $ABTS^{\bullet+}$.

Figure 4a shows the percentage scavenging activity of the biosynthesized nanocomposite and control (ascorbic acid) against ABTS. The straight line shows that with an increase in the concentration of the synthesized nanocomposite as well as ascorbic acid, the percentage scavenging activity increases, but the synthesized nanocomposite has a higher percentage scavenging activity than the control. The synthesized nanocomposite of CuO−ZnO and its antioxidant application were reported by Vibitha et al. (2020).[64] The reported nanoparticles from Azadirachta indica, Ocimum tenuiflourm, and aloe vera extract are examples that show the concentration dependence of the antioxidant activity, consistent with previous research.[62]

Figure 4b shows the percentage scavenging activity of the synthesized nanocomposite and ascorbic acid against DPPH. The straight line confirms that with an increase in the concentration of the synthesized nanocomposite as well as control, the percentage scavenging activity increases, but the nanocomposite exhibits a higher percentage scavenging activity than the control.

The 50% inhibitory concentration is a measure of the efficiency of a substance to inhibit a biological function. IC_{50} is the medication concentration required for half (50%) inhibition in vitro.[65]

The IC_{50} value of the synthesized nanocomposite (IC_{50} = 0.11) against DPPH and ABTS (0.512) was smaller than that of ascorbic acid (IC_{50} = 1.047). The low IC_{50} value suggested that the antioxidant potential of the synthesized nanocomposites was higher than that of ascorbic acid (IC_{50} = 1.04), which means that the synthesized nanocomposite exhibits excellent antioxidant activity against both DPPH and ABTS but higher in the case of DPPH than ABTS.[49] The current work proves the antioxidant activity of the synthesized CuO/NiO/ZnO nanocomposite and further establishes the fact that the CuO/ZnO/NiO nanocomposite has the potential to become the best scavenger in future clinical trials.

4. CONCLUSIONS

The green synthesis method used for the formation of the CuO/ZnO/NiO nanocomposite was proven to be one of the most effective and nontoxic routes. The antibacterial and antioxidant activities were found to be enhanced with an increase in the concentration of the ZnO/CuO/NiO nanocomposite, which might be due to the larger number of particles available to interact with free radicals and bacterial species. The as-synthesized CuO/NiO/ZnO nanocomposite was more effective against GPB (*S. aureus*) as compared to GNB (*E. coli*). The difference in the activity of the CuO/NiO/ZnO nanocomposite against both bacterial species is due to the difference in the cell wall composition and surface charge. Physiochemical properties of samples were examined through different characterization techniques such as UV−visible spectroscopy, SEM, FTIR spectroscopy, and XRD. The Tauc plot showed that the observed energy band gap of the synthesized nanocomposite was 3.8 eV. The XRD pattern obtained has sharp and intense peaks, which confirm the highly crystalline nature of the synthesized nanocomposite. The SEM micrograph showed that the background was highly agglomerated, where cavities were also observed at certain points. This is an indication that the *Dodonaea viscosa* leaf extract can be used for the synthesis of multimetallic nanocomposites with remarkable biological applications. The highest antioxidant

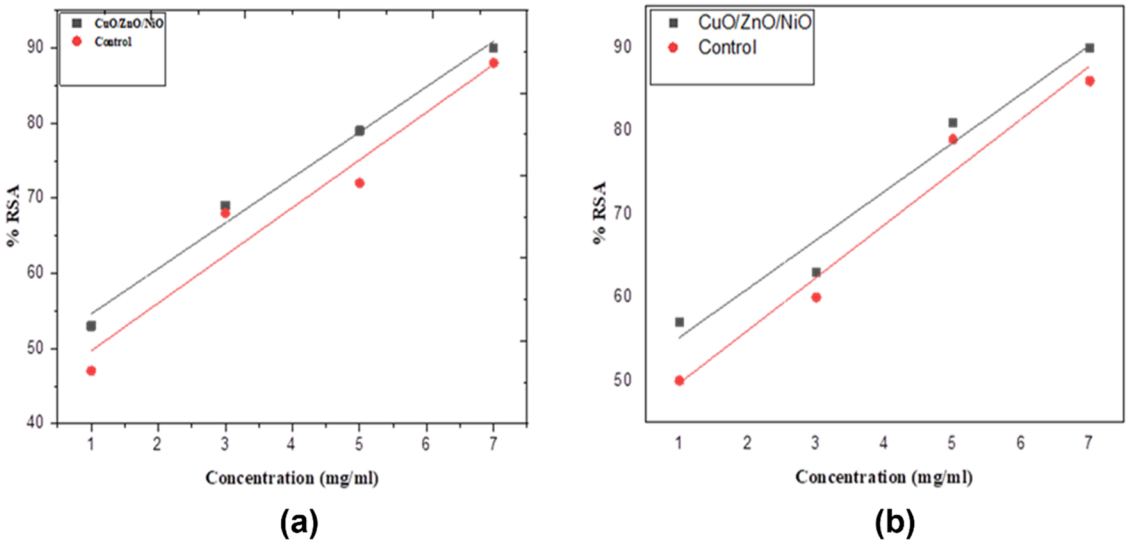

Figure 4. (a) ABTS assay and (b) DPPH assay showing the antioxidant activities of the synthesized CuO/ZnO/NiO nanocomposite and control (ascorbic acid).

https://doi.org/10.1021/acsomega.3c01896
ACS Omega 2023, 8, 21032−21041

efficiency may be attributed to the sub-30 nanometer size of the crystals, which is responsible for the large surface area.

AUTHOR INFORMATION

Corresponding Authors

Jahanzeb Khan − *Department of Chemistry, Mirpur University of Science and Technology (MUST), Mirpur, Azad Kashmir 10250, Pakistan; Department of Chemistry, University of Azad Jammu & Kashmir, Muzaffarabad, Azad Kashmir 13100, Pakistan*; Email: khanj10@tsinghua.org.cn

Davoud Dastan − *Department of Materials Science and Engineering, Cornell University, Ithaca, New York 14850, United States*; orcid.org/0000-0002-4124-5763; Email: d.dastan61@yahoo.com

Asad Syed − *Department of Botany and Microbiology, College of Science, King Saud University, Riyadh 11451, Saudi Arabia*; Email: assyed@ksu.edu.sa

Mustafa K. A. Mohammed − *College of Remote Sensing and Geophysics, Al-Karkh University of Science, Baghdad 10011, Iraq*; orcid.org/0000-0002-1850-6355; Email: mustafa_kareem97@yahoo.com

Authors

Saiqa Bibi − *Department of Chemistry, University of Azad Jammu & Kashmir, Muzaffarabad, Azad Kashmir 13100, Pakistan*

Irsa Naseem − *Department of Chemistry, University of Azad Jammu & Kashmir, Muzaffarabad, Azad Kashmir 13100, Pakistan*

Shakeel Ahmed − *College of Physics and Optoelectronic Engineering, Shenzhen University, Shenzhen 518060, P. R. China*

Muhammad Hafeez − *Department of Chemistry, University of Azad Jammu & Kashmir, Muzaffarabad, Azad Kashmir 13100, Pakistan*

Khalil Ahmed − *Department of Chemistry, Mirpur University of Science and Technology (MUST), Mirpur, Azad Kashmir 10250, Pakistan*

Faizah Altaf − *Department of Environmental Sciences, Women University of Azad Kashmir, Bagh 12500, Pakistan*

Majid S. Jabir − *Department of Applied Sciences, University of Technology-Iraq, 10011 Baghdad, Iraq*

Lin Tao − *School of Chemical Engineering, University of Science and Technology Liaoning, Anshan, Liaoning CN 114051, P. R. China*; orcid.org/0000-0002-3268-7009

Complete contact information is available at: https://pubs.acs.org/10.1021/acsomega.3c01896

Funding

This work is fully funded by the Higher Education Commission of Pakistan (HEC) under the Startup Research Grant Program, Project No. 298/IPFP-II(Batch-I)/SRGP/NAHE/HEC/2020/2.

Notes

The authors declare no competing financial interest.

ACKNOWLEDGMENTS

The authors extend their appreciation to the Higher Education Commission of Pakistan (HEC) for providing funds for our research work under the Startup Research Grant Program, Project No. 298/IPFP-II(Batch-I)/SRGP/NAHE/HEC/2020/2. The authors extend their appreciation to the Researchers Supporting Project number RSP2023R367, King Saud University, Riyadh, Saudi Arabia.

REFERENCES

(1) Haghnegahdar, N.; Abbasi Tarighat, M.; Dastan, D. Curcumin-functionalized nanocomposite AgNPs/SDS/MWCNTs for electrocatalytic simultaneous determination of dopamine, uric acid, and guanine in co-existence of ascorbic acid by glassy carbon electrode. *J. Mater. Sci.: Mater. Electron.* **2021**, *32*, 5602−5613.

(2) Fathinezhad, M.; AbbasiTarighat, M.; Dastan, D. Chemometrics heavy metal content clusters using electrochemical data of modified carbon paste electrode. *Environ. Nanotechnol. Monit. Management* **2020**, *14*, 1003.

(3) Meyers, M. A.; Mishra, A.; Benson, D. J. Mechanical properties of nanocrystalline materials. *Prog. Mater. Sci.* **2006**, *51*, 427−556.

(4) Ţălu, Ş.; Kulesza, S.; Bramowicz, M.; Stępień, K.; Dastan, D. Analysis of the Surface Microtexture of Sputtered Indium Tin Oxide Thin Films. *Arch. Metall. Mater.* **2021**, *66*, 443−450.

(5) Silva, J.P.B.; Sekhar, K.C.; Negrea, R.F.; Ghica, C.; Dastan, D.; Gomes, M.J.M. Ferroelectric properties of ZrO_2 films deposited on ITO-coated glass. *Ceram. Int.* **2022**, *48*, 6131−6137.

(6) Al Rugaie, O.; Jabir, M. S.; Mohammed, M.K.A.; Abbas, R. H.; Ahmed, D. S.; Sulaiman, G. M.; Mohammed, S.A.A.; Khan, R. A.; Al-Regaiey, K. A.; Alsharidah, M.; Mohany, K. M.; Mohammed, H. A. Modification of SWCNTs with hybrid materials ZnO−Ag and ZnO−Au for enhancing bactericidal activity of phagocytic cells against *Escherichia coli* through NOX2 pathway. *Sci. Rep.* **2022**, *12*, No. 17203.

(7) Dastan, D.; Shan, K.; Jafari, A.; Gity, F.; Yin, X.; Shi, Z.; Alharbi, N.; Reshi, B.; Fu, W.; Ţălu, Ş.; Aljerf, L.; Garmestani, H.; Ansari, L. Influence of nitrogen concentration on electrical, mechanical, and structural properties of tantalum nitride thin films prepared via DC magnetron sputtering. *Appl. Phys. A* **2022**, *128*, 400.

(8) Wei, S.; Shi, Z.; Wei, W.; Wang, H.; Dastan, D.; Huang, M.; Shi, J.; Chen, S. Facile preparation of ultralight porous carbon hollow nanoboxes for electromagnetic wave absorption. *Ceram. Int.* **2021**, *47*, 28014−28020.

(9) Mahmood, R. I.; Kadhim, A. A.; Ibraheem, S.; Albukhaty, S.; Mohammed-Salih, H. S.; Abbas, R. H.; Jabir, M. S.; Mohammed, M. K. A.; Nayef, U. M.; AlMalki, F. A.; Sulaiman, G. M.; Al-Karagoly, H. Biosynthesis of copper oxide nanoparticles mediated Annona muricata as cytotoxic and apoptosis inducer factor in breast cancer cell lines. *Sci. Rep.* **2022**, *12*, No. 16165.

(10) Al-Mousoi, A. K.; Mohammed, M.; Salih, S.; Pandey, R.; Madan, J.; Dastan, D.; Akman, E.; Alsewari, A.; Yaseen, Z. Comparative Study of the Correlation between Diffusion Length of Charge Carriers and the Performance of $CsSnGeI_3$ Perovskite Solar Cells. *Energy Fuels* **2022**, *36*, 14403−14410.

(11) Ashraf, I.; Ahmad, S.; Dastan, D.; Wang, C.; Garmestani, H.; Iqbal, M. Delaminated N-Ti3C2@Ni3S4 Nanocomposites based High-Performing Supercapacitor Device Fabrication. *Electrochim. Acta* **2023**, *442*, No. 141899.

(12) Shan, K.; Yi, Z.; Yin, X.; Dastan, D.; Altaf, F.; Garmestani, H.; Alamgir, F. Mixed Conductivity Evaluation and Sensing Characteristics of Limiting Current Oxygen Sensors. *Surf. Interfaces* **2020**, *21*, No. 100762.

(13) Ashraf, I.; Ahmad, S.; Dastan, D.; Wang, C.; Garmestani, H.; Iqbal, M. Fabrication of ionic liquid based D-Ti_3C_2/MoO_3 hybrid electrode system for efficient energy storage applications. *Electrochim. Acta* **2022**, *429*, No. 141036.

(14) Han, M.; Shi, Z.; Zhang, W.; Zhang, K.; Wang, H.; Dastan, D.; Fan, R. Significantly Enhanced High Permittivity and Negative Permittivity in Ag/Al_2O_3/3D-$BaTiO_3$/epoxy Metacomposites with Unique Hierarchical Heterogeneous Microstructures. *Composites, Part A* **2021**, *149*, No. 106559.

(15) Golinska, P.; Wypij, M.; Ingle, A. P.; Gupta, I.; Dahm, H.; Rai, M. Biogenic synthesis of metal nanoparticles from actinomycetes: biomedical applications and cytotoxicity. *Appl. Microbiol. Biotechnol.* **2014**, *98*, 8083−8097.

(16) Basnet, P.; Inakhunbi Chanu, T.; Samanta, D.; Chatterjee, S. A review on bio-synthesized zinc oxide nanoparticles using plant extracts as reductants and stabilizing agents. *J. Photochem. Photobiol. B Biol.* **2018**, *183*, 201−221.
(17) Dadi, R.; Azouani, R.; Traore, M.; Mielcarek, C.; Kanaev, A. Antibacterial activity of ZnO and CuO nanoparticles against gram positive and gram negative strains. *Mater. Sci. Eng. C* **2019**, *104*, No. 109968.
(18) Lobo, V.; Patil, A.; Phatak, A.; Chandra, N. Free radicals, antioxidants and functional foods: Impact on human health. *Pharmacogn. Rev.* **2010**, *4*, 118−126.
(19) Phaniendra, A.; Jestadi, D. B.; Periyasamy, L. Free Radicals: Properties, Sources, Targets, and Their Implication in Various Diseases. *Indian J. Clin. Biochem.* **2015**, *30*, 11−26.
(20) Haq, S.; Abbasi, F.; Ben Ali, M.; Hedfi, A.; Mezni, A.; Rehman, W.; Waseem, M.; Khan, A. R.; Shaheen, H. Green synthesis of cobalt oxide nanoparticles and the effect of annealing temperature on their physiochemical and biological properties. *Mater. Res. Express.* **2021**, *8*, 075009.
(21) Basavegowda, N.; Baek, K. H. Multimetallic nanoparticles as alternative antimicrobial agents: Challenges and perspectives. *Molecules* **2021**, *26*, 912.
(22) Pandya, S.; Universiy, P. Nanocomposites And It' S Application-Review Nanocomposites And It' S Application-Review - Shivani Pandya INTRODUCTION *ResearchGate* 2015, DOI: 10.13140/RG.2.1.2798.9840.
(23) Zhang, D.; Ma, X.; Gu, Y.; Huang, H.; Zhang, G. Green synthesis of metallic nanoparticles and their potential applications to treat cancer. *Front. Chem.* **2020**, *8*, 799.
(24) Shafey, A. M. El. Green synthesis of metal and metal oxide nanoparticles from plant leaf extracts and their applications: A review. *Green Process. Synth.* **2020**, *9*, 304−339.
(25) Naseer, M.; Aslam, U.; Khalid, B.; Chen, B. Green route to synthesize Zinc Oxide Nanoparticles using leaf extracts of *Cassia fistula* and Melia azadarach and their antibacterial potential. *Sci. Rep.* **2020**, *10*, No. 9055.
(26) Singh, J.; Dutta, T.; Kim, K. H.; Rawat, M.; Samddar, P.; Kumar, P. "Green" synthesis of metals and their oxide nanoparticles: Applications for environmental remediation. *J. Nanobiotechnol.* **2018**, *16*, 84.
(27) Faisal, S.; Jan, H.; Shah, S. A.; Shah, S.; Khan, A.; Akbar, M. T.; Rizwan, M.; Jan, F.; Wajidullah; Akhtar, N.; Khattak, A.; Syed, S. Green Synthesis of Zinc Oxide (ZnO) Nanoparticles Using Aqueous Fruit Extracts of Myristica fragrans: Their Characterizations and Biological and Environmental Applications. *ACS Omega* **2021**, *6*, 9709−9722.
(28) Sukumar, S.; Rudrasenan, A.; Padmanabhan Nambiar, D. Green-Synthesized Rice-Shaped Copper Oxide Nanoparticles Using Caesalpinia bonducella Seed Extract and Their Applications. *ACS Omega* **2020**, *5*, 1040−1051.
(29) Marslin, G.; Siram, K.; Maqbool, Q.; Selvakesavan, R. K.; Kruszka, D.; Kachlicki, P.; Franklin, G. Secondary metabolites in the green synthesis of metallic nanoparticles. *Materials* **2018**, *11*, 940.
(30) Dastan, D.; shan, K.; Jafari, A.; Marszalek, T.; Mohammed, M.; Tao, L.; Shi, Z.; Chen, Y.; Yin, X.; Alharbi, N.; Gity, F.; Asgary, S.; Hatamvand, M.; Ansari, L. Influence of heat treatment on H_2S gas sensing features of NiO thin films deposited via thermal evaporation technique. *Mater. Sci. Semicond. Process* **2023**, *154*, No. 107232.
(31) Naseem, T.; Durrani, T. The role of some important metal oxide nanoparticles for wastewater and antibacterial applications: A review. *Environ. Chem. Ecotoxicol.* **2021**, *3*, 59−75.
(32) Rajeshkumar, S.; Kumar, S. V.; Ramaiah, A.; Agarwal, H.; Lakshmi, T.; Roopan, S. M. Biosynthesis of zinc oxide nanoparticles using *Mangifera indica* leaves and evaluation of their antioxidant and cytotoxic properties in lung cancer (A549) cells. *Enzyme Microb. Technol.* **2018**, *117*, 91−95.
(33) Yin, X.-T.; Dastan, D.; Gity, F.; Li, J.; Shi, Z.; Alharbi, N.; Liu, Y.; Tan, X.; Gao, X.; Ma, X.; Ansari, L. Gas Sensing Selectivity of SnO_2-xNiO Sensors for Homogeneous Gases and its Selectivity Mechanism: Experimental and Theoretical Studies. *Sens. Actuators, A* **2023**, *354*, 114273.
(34) Yin, X.-T.; Li, J.; Wang, Q.; Dastan, D.; Shi, Z.-C.; Alharbi, N.; Garmestani, H.; Tan, X.-M.; Liu, Y.; Ma, X.-G. Opposite Sensing Response of Heterojunction Gas Sensors Based on SnO_2−Cr_2O_3 Nanocomposites to H_2 against CO and Its Selectivity Mechanism. *Langmuir* **2021**, *37*, 13548−13558.
(35) Ahmed, D. S.; Mohammed, B. K.; Mohammed, M.K.A. Long-term stable and hysteresis-free planar perovskite solar cells using green antisolvent strategy. *J. Mater. Sci.* **2021**, *56*, 15205−15214.
(36) Yin, X.-T.; Zhou, W.; Dastan, D.; Li, J.; Tan, X.; Liu, Y.; Gao, X.; Ma, X. Selectivity sensing response of ZnO-xCo_3O_4 based sensor to CO against CH_4. *Mater. Sci. Semicond. Process* **2022**, *149*, No. 106883.
(37) Zhou, W.; Dastan, D.; Yin, X.; Nie, S.; Wu, S.; Wang, Q.; Li, J. Optimization of gas sensing properties of n-SnO_2/pxCuO sensors for homogenous gases and the sensing mechanism. *J. Mater. Sci.: Mater. Electron.* **2020**, *31*, 18412−18426.
(38) Azam, A.; Ahmed, A. S.; Oves, M.; Khan, M. S.; Habib, S. S.; Memic, A. Antimicrobial activity of metal oxide nanoparticles against Gram-positive and Gram-negative bacteria: A comparative study. *Int. J. Nanomedicine* **2012**, *7*, 6003−6009.
(39) Singh, I. Plant Growth Promoting Rhizobacteria (PGPR) and their various mechanisms for plant growth enhancement in stressful conditions: a review. *Eur. J. Biol. Res.* **2018**, *8*, 191−213.
(40) Salinas-Sánchez, D. O.; Herrera-Ruiz, M.; Pérez, S.; Jiménez-Ferrer, E.; Zamilpa, A. Anti-inflammatory activity of hautriwaic acid isolated from *Dodonaea viscosa* leaves. *Molecules* **2012**, *17*, 4292−4299.
(41) Al-Snafi, A. E. A review on *Dodonaea viscosa*: A potential medicinal plant. *IOSR J. Pharm. (IOSRPHR)* **2017**, *07*, 10−21.
(42) Vaseghi, Z.; Tavakoli, O.; Nematollahzadeh, A. Rapid biosynthesis of novel Cu/Cr/Ni trimetallic oxide nanoparticles with antimicrobial activity. *J. Environ. Chem. Eng.* **2018**, *6*, 1898−1911.
(43) Sodeifian, G.; Sajadian, S. A.; Ardestani, N. S. Extraction of Dracocephalum kotschyi Boiss using supercritical carbon dioxide: experimental and optimization. *J. Supercrit. Fluids.* **2016**, *107*, 137−144.
(44) Sodeifian, G.; Ansari, K. Optimization of Ferulago Angulata oil extraction with supercritical carbon dioxide. *J. Supercrit. Fluids.* **2011**, *57*, 38−43.
(45) Sodeifian, G.; Ghorbandoost, S.; Sajadian, S. A.; Ardestani, N. S. Extraction of oil from Pistacia khinjuk using supercritical carbon dioxide: Experimental and modeling. *J. Supercrit. Fluids* **2016**, *110*, 265−274.
(46) Sodeifian, G.; Ardestani, N. S.; Sajadian, S. A.; Moghadamian, K. Properties of Portulaca oleracea seed oil via supercritical fluid extraction: Experimental and optimization. *J. Supercrit. Fluids* **2018**, *135*, 34−44.
(47) Sodeifian, G.; Ardestani, N. S.; Sajadian, S. A.; Panah, H. S. Experimental measurements and thermodynamic modeling of Coumarin-7 solid solubility in supercritical carbon dioxide: Production of nanoparticles via RESS method. *Fluid Phase Equilib.* **2019**, *483*, 122−143.
(48) Sodeifian, G.; Sajadian, S. A.; Ardestani, N. S.; Razmimanesh, F. Production of Loratadine drug nanoparticles using ultrasonic-assisted Rapid expansion of supercritical solution into aqueous solution (US-RESSAS). *J. Supercrit. Fluids.* **2019**, *147*, 241−253.
(49) Sodeifian, G.; Sajadian, S. A. Utilization of ultrasonic-assisted RESOLV (US-RESOLV) with polymeric stabilizers for production of amiodarone hydrochloride nanoparticles: Optimization of the process parameters. *Chem. Eng. Res. Des.* **2019**, *142*, 268−284.
(50) Sanchez-Hernandez, A. M.; Martin-Sanchez, N.; Sanchez-Montero, M. J.; Izquierdo, C.; Salvador, F. Different options to upgrade engine oils by gasification with steam and supercritical water. *J. Supercrit. Fluids* **2020**, *164*, No. 104912.
(51) Saadati Ardestani, N.; Sodeifian, G.; Sajadian, S. A. Preparation of phthalocyanine green nano pigment using supercritical CO2 gas

antisolvent (GAS): experimental and modeling. *Heliyon* **2020**, *6*, No. e04947.
(52) Sodeifian, G.; Sajadian, S. A.; Derakhsheshpour, R. CO2 utilization as a supercritical solvent and supercritical antisolvent in production of sertraline hydrochloride nanoparticles. *J. CO2 Util.* **2022**, *55*, No. 101799.
(53) Fathi, M.; Sodeifian, G.; Sajadian, S. A. Experimental study of ketoconazole impregnation into polyvinyl pyrrolidone and hydroxyl propyl methyl cellulose using supercritical carbon dioxide: Process optimization. *J. Supercrit. Fluids* **2022**, *188*, No. 105674.
(54) Haq, S.; Raja, A. W.; Rehman, S. U.; Mezni, A.; Ben Ali, M.; Hedfi, A.; Shahzad, M. I.; Rehman, W.; Shahzad, N.; Waseem, M.; Ahmad, P. Phytogenic Synthesis and Characterization of NiO-ZnO Nanocomposite for the Photodegradation of Brilliant Green and 4-Nitrophenol. *J. Chem.* **2021**, *2021*, 1−10.
(55) Khan, J.; Ilyas, S.; Akram, B.; Ahmad, K.; Hafeez, M.; Siddiq, M.; Aqeel, M. Zno / NiO coated multi-walled carbon nanotubes for textile dyes degradation. *Arab. J. Chem.* **2018**, *11*, 880−896.
(56) Khan, J.; Naseem, I.; Bibi, S.; Ahmad, S.; Altaf, F.; Hafeez, M.; Almoneef, M. M.; Ahmad, K. Green Synthesis of Silver Nanoparticles (Ag-NPs) Using Debregeasia Salicifolia for Biological Applications. *Materials* **2023**, *16*, 129.
(57) Ahmed, D. S.; Mohammed, M.K.A. Studying the bactericidal ability and biocompatibility of gold and gold oxide nanoparticles decorating on multi-wall carbon nanotubes. *Chem. Papers* **2020**, *74*, 4033−4046.
(58) Luan, B.; Liu, C.; Chen, P.; Chen, R. Nanotechnology Reviews " Just Accepted" Papers *Nanotechnol. Rev.* 2011.
(59) Shi, L.-B.; Tang, P. F.; Zhang, W.; Zhao, Y. P.; Zhang, L. C.; Zhang, H. Green synthesis of CuO nanoparticles using Cassia auriculata leaf extract and in vitro evaluation of their biocompatibility with rheumatoid arthritis macrophages (RAW 264.7). *Trop. J. Pharm. Res.* **2017**, *16*, 185.
(60) Fallah, M.; Zamani-Meymian, M.; Rabbani, M. Influence of two gradual steps of vacuum annealing on structural and opto-electronic characteristics of Nb-doped TiO2 transparent conducting oxide. *Superlattices Microstruct.* **2018**, *123*, 242−250.
(61) Sakthivel, P.; Anandha babu, G.; Karuppiah, M.; Asaithambi, S.; Balaji, V.; Pandian, M. S.; Ramasamy, P.; Mohammed, M. K. A.; Navaneethan, N.; Ravi, G. Electrochemical energy storage applications of carbon nanotube supported heterogeneous metal sulfide electrodes. *Ceram. Int.* **2022**, *48*, 6157−6165.
(62) Al-Mousoi, A. K.; Mohammed, M.K.A.; Khalaf, H. A. Preparing and characterization of indium arsenide (InAs) thin films by chemical spray pyrolysis (CSP) technique. *Optik* **2016**, *127*, 5834−5840.
(63) Shabestarian, H.; Homayouni-Tabrizi, M.; Soltani, M.; Namvar, F.; Azizi, S.; Mohamad, R.; Shabestarian, H. Green Synthesis of Gold Nanoparticles Using Sumac Aqueous Extract and Their Antioxidant Activity. *Mater. Res.* **2017**, *20*, 264−270.
(64) Noohpisheh, Z.; Amiri, H.; Farhadi, S.; Mohammadi-Gholami, A. Green synthesis of Ag-ZnO nanocomposites using Trigonella foenum-graecum leaf extract and their antibacterial, antifungal, antioxidant and photocatalytic properties. *Spectrochim. Acta, Part A* **2020**, *240*, No. 118595.
(65) Safajou, H.; Ghanbari, M.; Amiri, O.; Khojasteh, H.; Namvar, F.; Zinatloo-Ajabshir, S.; Salavati-Niasari, M. Green synthesis and characterization of RGO/Cu nanocomposites as photocatalytic degradation of organic pollutants in waste-water. *Int. J. Hydrogen Energy* **2021**, *46*, 20534−20546.
(66) Mohammed, M. K. A.; Jabir, M. S.; Abdulzahraa, H. G.; Mohammed, S. H.; Al-Azzawi, W. K.; Ahmed, D. S.; Singh, S.; Kumar, A.; Asaithambi, S.; Shekargoftar, M. Introduction of cadmium chloride additive to improve the performance and stability of perovskite solar cells. *RSC Adv.* **2022**, *12*, 20461−20470.
(67) Humadi, M. D.; Hussein, H. T.; Mohamed, M. S.; Mohammed, M.K.A.; Kayahan, E. A facile approach to improve the performance and stability of perovskite solar cells via FA/MA precursor temperature controlling in sequential deposition fabrication. *Optical Mater.* **2021**, *112*, No. 110794.
(68) Altaf, F.; Ahmed, S.; Dastan, D.; Batool, R.; Rehman, Z. U.; Shi, Z.; Hameed, M. U.; Bocchetta, P.; Jacob, K. Novel sepiolite reinforced emerging composite polymer electrolyte membranes for high-performance direct methanol fuel cells. *Mater. Today Chem.* **2022**, *24*, No. 100843.
(69) Liang, L.; Shi, Z.; Tan, X.; Sun, S.; Chen, M.; Dastan, D.; Dong, B.; Cao, L. Largely Improved Breakdown Strength and Discharge Efficiency of Layer-Structured Nanocomposites by Filling with a Small Loading Fraction of 2D Zirconium Phosphate Nanosheets. *Adv. Mater. Interfaces* **2022**, *9*, No. 2101646.
(70) Yin, X.-T.; Huang, H.; Xie, J.; Dastan, D.; Li, J.; Liu, Y.; Tan, X.; Gao, X.; Shah, W.; Ma, X. High-performance visible-light active Sr-doped porous $LaFeO_3$ semiconductor prepared via sol−gel method. *Green Chem. Lett. Rev.* **2022**, *15*, 546−556.
(71) Timoumi, A.; Dastan, D.; Jamoussi, B.; Essalah, K.; Alsalmi, O.; Bouguila, N.; Abassi, H.; Chakroun, R.; Shi, Z.; Ţălu, Ş. Experimental and Theoretical Studies on Optical Properties of Tetra(Imidazole) of Palladium (II) Phthalocyanine. *Molecules* **2022**, *27*, 6151.
(72) Soleimany, A.; Khoee, S.; Dastan, D.; Shi, Z.; Yu, S.; Sarmento, B. Two-photon photodynamic therapy based on FRET using tumor-cell targeted riboflavin conjugated graphene quantum dot. *J. Photochem. & Photobiol., B: Biol.* **2023**, *238*, No. 112602.
(73) Abbasi, S.; Dastan, D.; Ţălu, Ş.; Tahir, M. B.; Elias, M.; Tao, L.; Li, Z. Evaluation of the dependence of methyl orange organic pollutant removal rate on the amount of titanium dioxide nanoparticles in MWCNTs-TiO2 photocatalyst using statistical methods and Duncan's multiple range test. *Int. J. Environ. Anal. Chem.* **2022**, 1−15.
(74) Jayakrishnan, A.; Silva, J.; Kamakshi, K.; Dastan, D.; Annapureddy, V.; Pereira, M.; Sekhar, K. Are lead-free relaxor ferroelectric materials the most promising candidates for energy storage capacitors? *Prog. Mater. Sci.* **2023**, *132*, No. 101046.
(75) Zhang, Y.; Mahdavi, B.; Mohammadhosseini, M.; Rezaei-Seresht, E.; Paydarfard, S.; Qorbani, M.; Karimian, M.; Abbasi, N.; Ghaneialvar, H.; Karimi, E. Green synthesis of NiO nanoparticles using Calendula officinalis extract: Chemical charactrization, anti-oxidant, cytotoxicity, and anti-esophageal carcinoma properties. *Arab. J. Chem.* **2021**, *14*, No. 103105.
(76) Juma, A. O.; Arbab, E.A.A.; Muiva, C. M.; Lepodise, L. M.; Mola, G. T. Synthesis and characterization of CuO-NiO-ZnO mixed metal oxide nanocomposite. *J. Alloys Compd.* **2017**, *723*, 866−872.
(77) Hafeez, M.; Arshad, R.; Khan, J.; Akram, B.; Ahmad, M. N.; Hameed, M. U.; Haq, S. Populus ciliata mediated synthesis of copper oxide nanoparticles for potential biological applications. *Mater. Res. Express.* **2019**, *6*, 055043.
(78) Paul, D.; Mangla, S.; Neogi, S. Antibacterial study of CuO-NiO-ZnO trimetallic oxide nanoparticle. *Mater. Lett.* **2020**, *271*, No. 127740.
(79) Tao, L.; Dastan, D.; Wang, W.; Poldorn, P.; Meng, X.; Wu, M.; Zhao, H.; Zhang, H.; Li, L.; An, B. Metal-Decorated InN Monolayer Senses N2 against CO2. *ACS Appl. Mater. Interfaces* **2023**, *15*, 12534−12544.
(80) Moradi-Haji Jafan, M.; Zamani-Meymian, M.; Rahimi, R.; Rabbani, M. Effect of pyrolysis temperature on the electrical, optical, structural, and morphological properties of ITO thin films prepared by a sol−gel spin coating process. *Microelectron. Eng.* **2014**, *130*, 40−45.
(81) Jafan, M.; Zamani-Meymian, M.; Rahimi, R.; Rabbani, M. The effect of solvents and the thickness on structural, optical and electrical properties of ITO thin films prepared by a sol−gel spin-coating process. *J. Nanostruct. Chem.* **2014**, *4*, 89.
(82) Chenab, K.; Sohrabi, B.; Zamani-Meymian, M. Cobalt complex dye as a novel sensitizer in dye sensitized solar cells. *Mater. Res. Express* **2020**, *6*, No. 125536.
(83) Potbhare, A. K.; Chaudhary, R.; Chouke, P.; Yerpude, S.; Mondal, A.; Sonkusare, V.; Rai, A.; Junej, H. Phytosynthesis of nearly monodisperse CuO nanospheres using Phyllanthus reticulatus/Conyza bonariensis and its antioxidant/antibacterial assays. *Mater. Sci. Eng., C* **2019**, *99*, 783−793.

https://doi.org/10.1021/acsomega.3c01896
ACS Omega 2023, 8, 21032−21041

(84) Li, H.; Wang, X.; Gong, Y.; Zhao, H.; Liu, Z.; Tao, L.; Peng, Y.; Ma, K.; Hu, Z.; Dastan, D. Polyimide/crown ether composite film with low dielectric constant and low dielectric loss for high signal transmission. *RSC Adv.* **2023**, *13*, 7585.
(85) Mohammed, M. K. A.; Al-Mousoi, A.; Majeed, S.; Singh, S.; Kumar, A.; Pandey, R.; Madan, J.; Ahmed, D.; Dastan, D. Stable Hole-Transporting Material-Free Perovskite Solar Cells with Efficiency Exceeding 14% via the Introduction of a Malonic Acid Additive for a Perovskite Precursor. *Energy Fuels* **2022**, *36*, 13187−13194.
(86) Mohammed, M.; Al-Mousoi, A.; Singh, S.; Younis, U.; Kumar, A.; Dastan, D.; Ravi, G. Ionic Liquid Passivator for Mesoporous Titanium Dioxide Electron Transport Layer to Enhance Efficiency and Stability of Hole Conductor-Free Perovskite Solar Cells. *Energy Fuels* **2022**, *36*, 12192−12200.
(87) Akram, B.; Ahmad, K.; Khan, J.; Khan, B. A.; Akhtar, J. Low-temperature solution-phase route to sub-10 nm titanium oxide nanocrystals having super-enhanced photoreactivity. *New J. Chem.* **2018**, *42*, 10947−10952.
(88) Zhu, P.; Dastan, D.; Liu, L.; Wu, L.; Shi, Z.; Chu, Q.; Altaf, F.; Mohammed, M. Surface wettability of various phases of titania thin films: Atomic-scale simulation studies. *J. Mol. Graph. Model.* **2023**, *118*, No. 108335.
(89) Ashraf, I.; Ahmad, S.; Nazir, F.; Dastan, D.; Shi, Z.; Garmestani, H.; Iqbal, M. Hydrothermal synthesis and water splitting application of d-Ti3C2 MXene/V2O5 hybrid nanostructures as an efficient bifunctional catalyst. *Int. J. Hydrogen Energy* **2022**, *47*, 27383−27396.
(90) Dlugaszewska, J.; Dobrucka, R. Effectiveness of biosynthesized trimetallic Au/Pt/Ag nanoparticles on planktonic and biofilm Enterococcus faecalis and Enterococcus faecium forms. *J. Clust. Sci.* **2019**, *30*, 1091−1101.
(91) Tan, G.-L.; Tang, D.; Dastan, D.; Jafari, A.; Shi, Z.; Chu, Q.; Silva, J.; Yin, X. Structures, Morphological Control, and Antibacterial Performance of Tungsten Oxide Thin Films. *Ceram. Int.* **2021**, *47*, 17153−17160.
(92) Mohammadi-Aloucheh, R.; Habibi-Yangjeh, A.; Bayrami, A.; Latifi-Navid, S.; Asadi, A. Green synthesis of ZnO and ZnO/CuO nanocomposites in Mentha longifolia leaf extract: characterization and their application as anti-bacterial agents. *J. Mater. Sci. Mater. Electron.* **2018**, *29*, 13596−13605.
(93) Nasrollahzadeh, M.; Sajjadi, M.; Iravani, S.; Varma, R. S. Trimetallic nanoparticles: greener synthesis and their applications. *Nanomaterials* **2020**, *10*, 1784.
(94) Manikandan, V.; Velmurugan, P.; Park, J. H.; Lovanh, N.; Seo, S. K.; Jayanthi, P.; Park, Y. J.; Cho, M.; Oh, B. T. Synthesis and antimicrobial activity of palladium nanoparticles from Prunus × yedoensis leaf extract. *Mater. Lett.* **2016**, *185*, 335−338.
(95) Srihasam, S.; Thyagarajan, K.; Korivi, M.; Lebaka, V. R.; Mallem, S.P.R. Phytogenic generation of NiO nanoparticles using Stevia leaf extract and evaluation of their in-vitro antioxidant and antimicrobial properties. *Biomolecules* **2020**, *10*, 89.
(96) Amin, F.; Khattak, B.; Alotaibi, A.; Qasim, M.; Ahmad, I.; Ullah, R.; Bourhia, M.; Gul, A.; Zahoor, S.; Ahmad, R. Green synthesis of copper oxide nanoparticles using Aerva javanica leaf extract and their characterization and investigation of in vitro antimicrobial potential and cytotoxic activities. *Evidence-Based Complement. Altern. Med.* **2021**, *2021*, 1−12.
(97) Suresh, D.; Nethravathi, P. C.; Rajanaika, H.; Nagabhushana, H.; Sharma, S. C. Green synthesis of multifunctional zinc oxide (ZnO) nanoparticles using *Cassia fistula* plant extract and their photodegradative, antioxidant and antibacterial activities. *Mater. Sci. Semicond. Process.* **2015**, *31*, 446−454.
(98) Sowmiya, F.; Brintha, S. R. Synthesis and Characterization of Zno-Cdo Nanocomposite and Its Antibacterial Activity. *J. Pharm. Negat. Results* **2022**, *13*, 3559−3569.
(99) Chen, W.; Yue, L.; Jiang, Q.; Liu, X.; Xia, W. Synthesis of varisized chitosan-selenium nanocomposites through heating treatment and evaluation of their antioxidant properties. *Int. J. Biol. Macromol.* **2018**, *114*, 751−758.
(100) Vibitha, B. V.; Anitha, B.; Krishna, P.G.A.; Tharayil, J. N. *Plant Extracts Assisted Synthesis, Characterization and Antioxidant Properties of ZnO: CuO Nanocomposites*, AIP Conference Proceedings, AIP Publishing LLC, 2020; p 70037.
(101) Hajji, S.; Salem, R.B.S.-B.; Hamdi, M.; Jellouli, K.; Ayadi, W.; Nasri, M.; Boufi, S. Nanocomposite films based on chitosan−poly (vinyl alcohol) and silver nanoparticles with high antibacterial and antioxidant activities. *Process Saf. Environ. Prot.* **2017**, *111*, 112−121.
(102) Siriwong, P.; Thongtem, T.; Phuruangrat, A.; Thongtem, S. Hydrothermal synthesis, characterization, and optical properties of wolframite ZnWO4nanorods. *CrystEngComm* **2011**, *13*, 1564−1569.
(103) Pinchujit, S.; Phuruangrat, A.; Wannapop, S.; Sakhon, T.; Kuntalue, B.; Thongtem, T.; Thongtem, S. Synthesis and characterization of heterostructure Pt/Bi2WO6 nanocomposites with enhanced photodegradation efficiency induced by visible radiation. *Solid State Sci.* **2022**, *134*, No. 107064.
(104) Yayapao, O.; Thongtem, T.; Phuruangrat, A.; Thongtem, S. Synthesis and characterization of highly efficient Gd doped ZnO photocatalyst irradiated with ultraviolet and visible radiations. *Mater. Sci. Semicond. Process.* **2015**, *39*, 786−792.
(105) Liu, Y.; Li, X.; Li, X.; Shao, C.; Han, C.; Xin, J.; Lu, D.; Niu, L.; Tang, Y.; Liu, Y. Highly permeable WO3/CuWO4 heterostructure with 3D hierarchical porous structure for high-sensitive room-temperature visible-light driven gas sensor. *Sens. Actuators, B* **2022**, *365*, No. 131926.
(106) Liu, Y.; Wong, T.; Huang, X.; Yiu, C.; Gao, Y.; Zhao, L.; Zhou, J.; Park, W.; Zhao, Z.; Yao, K.; Li, H.; Jia, H.; Li, J.; Li, J.; Huang, Y.; Wu, M.; Zhang, B.; Li, D.; Zhang, C.; Wang, Z.; Yu, X. Skin-integrated, stretchable, transparent triboelectric nanogenerators based on ion-conducting hydrogel for energy harvesting and tactile sensing. *Nano Energy* **2022**, *99*, No. 107442.
(107) Sen, S. K.; Munshi, M.; Kumar, A.; Mortuza, A.; Manir, M.; Islam, M.; Hossain, M.; Hossain, M. Structural, optical, magnetic, and enhanced antibacterial properties of hydrothermally synthesized Sm-incorporating α-MoO3 2D-layered nanoplates. *RSC Adv.* **2022**, *12*, 34584−34600.
(108) Verma, N.; Kumar, N. Synthesis and Biomedical Applications of Copper Oxide Nanoparticles: An Expanding Horizon. *ACS Biomater. Sci. Eng.* **2019**, *5*, 1170−1188.
(109) Pervez, M.; Mia, M.; Hossain, S.; Saha, S.; Ali, M.; Sarker, P.; Hossain, M.; Matin, M.; Hoq, M.; Chowdhury, M. Influence of total absorbed dose of gamma radiation on optical bandgap and structural properties of Mg-doped zinc oxide. *Optik* **2018**, *162*, 140−150.

https://doi.org/10.1021/acsomega.3c01896
ACS Omega 2023, 8, 21032−21041